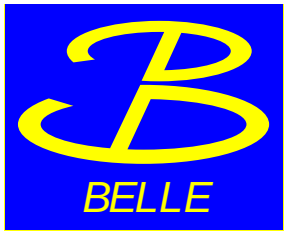

BELLE-CONF-0508
EPS05-480

A High Statistics Study of the Decay $\tau^- \to \pi^- \pi^0 \nu_\tau$

K. Abe,[9] K. Abe,[48] I. Adachi,[9] H. Aihara,[50] K. Aoki,[24] K. Arinstein,[2] Y. Asano,[55] T. Aso,[54] V. Aulchenko,[2] T. Aushev,[14] T. Aziz,[46] S. Bahinipati,[5] A. M. Bakich,[45] V. Balagura,[14] Y. Ban,[37] S. Banerjee,[46] E. Barberio,[23] M. Barbero,[8] A. Bay,[20] I. Bedny,[2] K. Belous,[12] U. Bitenc,[15] I. Bizjak,[15] S. Blyth,[26] A. Bondar,[2] A. Bozek,[30] M. Bračko,[9,22,15] J. Brodzicka,[30] T. E. Browder,[8] M.-C. Chang,[49] P. Chang,[29] Y. Chao,[29] A. Chen,[26] K.-F. Chen,[29] W. T. Chen,[26] B. G. Cheon,[4] C.-C. Chiang,[29] R. Chistov,[14] S.-K. Choi,[7] Y. Choi,[44] Y. K. Choi,[44] A. Chuvikov,[38] S. Cole,[45] J. Dalseno,[23] M. Danilov,[14] M. Dash,[57] L. Y. Dong,[11] R. Dowd,[23] J. Dragic,[9] A. Drutskoy,[5] S. Eidelman,[2] Y. Enari,[24] D. Epifanov,[2] F. Fang,[8] S. Fratina,[15] H. Fujii,[9] M. Fujikawa,[25] N. Gabyshev,[2] A. Garmash,[38] T. Gershon,[9] A. Go,[26] G. Gokhroo,[46] P. Goldenzweig,[5] B. Golob,[21,15] A. Gorišek,[15] M. Grosse Perdekamp,[39] H. Guler,[8] R. Guo,[27] J. Haba,[9] K. Hara,[9] T. Hara,[35] Y. Hasegawa,[43] N. C. Hastings,[50] K. Hasuko,[39] K. Hayasaka,[24] H. Hayashii,[25] M. Hazumi,[9] T. Higuchi,[9] L. Hinz,[20] T. Hojo,[35] T. Hokuue,[24] Y. Hoshi,[48] K. Hoshina,[53] S. Hou,[26] W.-S. Hou,[29] Y. B. Hsiung,[29] Y. Igarashi,[9] T. Iijima,[24] K. Ikado,[24] A. Imoto,[25] K. Inami,[24] A. Ishikawa,[9] H. Ishino,[51] K. Itoh,[50] R. Itoh,[9] M. Iwasaki,[50] Y. Iwasaki,[9] C. Jacoby,[20] C.-M. Jen,[29] R. Kagan,[14] H. Kakuno,[50] J. H. Kang,[58] J. S. Kang,[17] P. Kapusta,[30] S. U. Kataoka,[25] N. Katayama,[9] H. Kawai,[3] N. Kawamura,[1] T. Kawasaki,[32] S. Kazi,[5] N. Kent,[8] H. R. Khan,[51] A. Kibayashi,[51] H. Kichimi,[9] H. J. Kim,[19] H. O. Kim,[44] J. H. Kim,[44] S. K. Kim,[42] S. M. Kim,[44] T. H. Kim,[58] K. Kinoshita,[5] N. Kishimoto,[24] S. Korpar,[22,15] Y. Kozakai,[24] P. Križan,[21,15] P. Krokovny,[9] T. Kubota,[24] R. Kulasiri,[5] C. C. Kuo,[26] H. Kurashiro,[51] E. Kurihara,[3] A. Kusaka,[50] A. Kuzmin,[2] Y.-J. Kwon,[58] J. S. Lange,[6] G. Leder,[13] S. E. Lee,[42] Y.-J. Lee,[29] T. Lesiak,[30] J. Li,[41] A. Limosani,[9] S.-W. Lin,[29] D. Liventsev,[14] J. MacNaughton,[13] G. Majumder,[46] F. Mandl,[13] D. Marlow,[38] H. Matsumoto,[32] T. Matsumoto,[52] A. Matyja,[30] Y. Mikami,[49] W. Mitaroff,[13] K. Miyabayashi,[25] H. Miyake,[35] H. Miyata,[32] Y. Miyazaki,[24] R. Mizuk,[14] D. Mohapatra,[57] G. R. Moloney,[23] T. Mori,[51] A. Murakami,[40] T. Nagamine,[49] Y. Nagasaka,[10] T. Nakagawa,[52] I. Nakamura,[9] E. Nakano,[34] M. Nakao,[9] H. Nakazawa,[9] Z. Natkaniec,[30] K. Neichi,[48] S. Nishida,[9] O. Nitoh,[53] S. Noguchi,[25] T. Nozaki,[9] A. Ogawa,[39] S. Ogawa,[47] T. Ohshima,[24] T. Okabe,[24] S. Okuno,[16] S. L. Olsen,[8] Y. Onuki,[32] W. Ostrowicz,[30] H. Ozaki,[9] P. Pakhlov,[14] H. Palka,[30] C. W. Park,[44] H. Park,[19] K. S. Park,[44] N. Parslow,[45] L. S. Peak,[45] M. Pernicka,[13] R. Pestotnik,[15] M. Peters,[8] L. E. Piilonen,[57] A. Poluektov,[2] F. J. Ronga,[9] N. Root,[2] M. Rozanska,[30] H. Sahoo,[8] M. Saigo,[49] S. Saitoh,[9] Y. Sakai,[9] H. Sakamoto,[18] H. Sakaue,[34] T. R. Sarangi,[9] M. Satapathy,[56] N. Sato,[24] N. Satoyama,[43] T. Schietinger,[20] O. Schneider,[20] P. Schönmeier,[49] J. Schümann,[29] C. Schwanda,[13] A. J. Schwartz,[5] T. Seki,[52] K. Senyo,[24] R. Seuster,[8] M. E. Sevior,[23] M. Shapkin,[12] T. Shibata,[32] H. Shibuya,[47] J.-G. Shiu,[29]

B. Shwartz,[2] V. Sidorov,[2] J. B. Singh,[36] A. Sokolov,[12] A. Somov,[5] N. Soni,[36] R. Stamen,[9] S. Stanič,[33] M. Starič,[15] A. Sugiyama,[40] K. Sumisawa,[9] T. Sumiyoshi,[52] S. Suzuki,[40] S. Y. Suzuki,[9] O. Tajima,[9] N. Takada,[43] F. Takasaki,[9] K. Tamai,[9] N. Tamura,[32] K. Tanabe,[50] M. Tanaka,[9] G. N. Taylor,[23] Y. Teramoto,[34] X. C. Tian,[37] K. Trabelsi,[8] Y. F. Tse,[23] T. Tsuboyama,[9] T. Tsukamoto,[9] K. Uchida,[8] Y. Uchida,[9] S. Uehara,[9] T. Uglov,[14] K. Ueno,[29] Y. Unno,[9] S. Uno,[9] P. Urquijo,[23] Y. Ushiroda,[9] G. Varner,[8] K. E. Varvell,[45] S. Villa,[20] C. C. Wang,[29] C. H. Wang,[28] M.-Z. Wang,[29] M. Watanabe,[32] Y. Watanabe,[51] L. Widhalm,[13] C.-H. Wu,[29] Q. L. Xie,[11] B. D. Yabsley,[57] A. Yamaguchi,[49] H. Yamamoto,[49] S. Yamamoto,[52] Y. Yamashita,[31] M. Yamauchi,[9] Heyoung Yang,[42] J. Ying,[37] S. Yoshino,[24] Y. Yuan,[11] Y. Yusa,[49] H. Yuta,[1] S. L. Zang,[11] C. C. Zhang,[11] J. Zhang,[9] L. M. Zhang,[41] Z. P. Zhang,[41] V. Zhilich,[2] T. Ziegler,[38] and D. Zürcher[20]

(The Belle Collaboration)

[1]*Aomori University, Aomori*
[2]*Budker Institute of Nuclear Physics, Novosibirsk*
[3]*Chiba University, Chiba*
[4]*Chonnam National University, Kwangju*
[5]*University of Cincinnati, Cincinnati, Ohio 45221*
[6]*University of Frankfurt, Frankfurt*
[7]*Gyeongsang National University, Chinju*
[8]*University of Hawaii, Honolulu, Hawaii 96822*
[9]*High Energy Accelerator Research Organization (KEK), Tsukuba*
[10]*Hiroshima Institute of Technology, Hiroshima*
[11]*Institute of High Energy Physics, Chinese Academy of Sciences, Beijing*
[12]*Institute of High Energy Physics, Protvino*
[13]*Institute of High Energy Physics, Vienna*
[14]*Institute for Theoretical and Experimental Physics, Moscow*
[15]*J. Stefan Institute, Ljubljana*
[16]*Kanagawa University, Yokohama*
[17]*Korea University, Seoul*
[18]*Kyoto University, Kyoto*
[19]*Kyungpook National University, Taegu*
[20]*Swiss Federal Institute of Technology of Lausanne, EPFL, Lausanne*
[21]*University of Ljubljana, Ljubljana*
[22]*University of Maribor, Maribor*
[23]*University of Melbourne, Victoria*
[24]*Nagoya University, Nagoya*
[25]*Nara Women's University, Nara*
[26]*National Central University, Chung-li*
[27]*National Kaohsiung Normal University, Kaohsiung*
[28]*National United University, Miao Li*
[29]*Department of Physics, National Taiwan University, Taipei*
[30]*H. Niewodniczanski Institute of Nuclear Physics, Krakow*
[31]*Nippon Dental University, Niigata*
[32]*Niigata University, Niigata*

[33]Nova Gorica Polytechnic, Nova Gorica
[34]Osaka City University, Osaka
[35]Osaka University, Osaka
[36]Panjab University, Chandigarh
[37]Peking University, Beijing
[38]Princeton University, Princeton, New Jersey 08544
[39]RIKEN BNL Research Center, Upton, New York 11973
[40]Saga University, Saga
[41]University of Science and Technology of China, Hefei
[42]Seoul National University, Seoul
[43]Shinshu University, Nagano
[44]Sungkyunkwan University, Suwon
[45]University of Sydney, Sydney NSW
[46]Tata Institute of Fundamental Research, Bombay
[47]Toho University, Funabashi
[48]Tohoku Gakuin University, Tagajo
[49]Tohoku University, Sendai
[50]Department of Physics, University of Tokyo, Tokyo
[51]Tokyo Institute of Technology, Tokyo
[52]Tokyo Metropolitan University, Tokyo
[53]Tokyo University of Agriculture and Technology, Tokyo
[54]Toyama National College of Maritime Technology, Toyama
[55]University of Tsukuba, Tsukuba
[56]Utkal University, Bhubaneswer
[57]Virginia Polytechnic Institute and State University, Blacksburg, Virginia 24061
[58]Yonsei University, Seoul

Abstract

We report a measurement of the branching fraction for $\tau^- \to \pi^-\pi^0\,\nu_\tau$ and the invariant mass spectrum of the resulting $\pi^-\pi^0$ system using 72.2 fb^{-1} of data recorded by the Belle detector at the KEKB e^+e^- collider. The branching fraction obtained is $(25.15 \pm 0.04 \pm 0.31)\%$, where the first error is statistical and the second is systematic. The unfolded $\pi^-\pi^0$ mass spectrum is used to determine resonance parameters for the $\rho(770)$, $\rho'(1450)$, and $\rho''(1700)$ mesons. We also use this spectrum to estimate the hadronic contribution to the anomalous magnetic moment of the muon.

PACS numbers: 13.40.Gp, 13.35.Dx, 14.60.Fg

INTRODUCTION

Among the decay channels of the τ lepton, $\tau^- \to \pi^-\pi^0\,\nu_\tau$ has the largest branching fraction. The decay is dominated by intermediate resonances and thus provides information on the properties of the $\rho(770)$, $\rho'(1450)$, and $\rho''(1700)$ mesons and their interference. Since leptons do not participate in the strong interaction, hadronic τ decays provide a clean environment for studying the dynamics of hadronic states in an interesting energy range dominated by resonances.

Under the Conserved Vector Current (CVC) theorem, the $\pi^-\pi^0$ mass spectrum in this range can be used to improve the theoretical error on the anomalous magnetic moment of the muon $a_\mu = (g_\mu - 2)/2$. A recent review of the calculations of a_μ is given in Ref. [1]. It is known that the theoretical error on a_μ is dominated by the (leading-order) hadronic contribution $a_\mu^{\rm had,LO}$, given by the hadronic vacuum polarization. This contribution cannot be evaluated within the framework of perturbative QCD; however, it can be evaluated from a measurement of the cross section for e^+e^- annihilation to hadrons [2, 3]. Alternatively, CVC relates the properties of the $\pi^+\pi^-$ system produced in $e^+e^- \to \pi^+\pi^-$ to those of the $\pi^-\pi^0$ system produced in $\tau^-\to\pi^-\pi^0\,\nu_\tau$ decay; thus, using CVC and correcting for isospin-violating effects, τ data have also been used to obtain a more precise prediction for $a_\mu^{\rm had,LO}$ [2, 4].

Recently, data on $e^+e^-\to\pi^+\pi^-$ has become available from the CMD-2, KLOE, and SND experiments [5, 6, 7, 8]. Data on τ decays is available from the ALEPH [9, 10], CLEO [11], and OPAL [12] experiments. The most recent evaluation of the hadronic contribution to a_μ using e^+e^- data gives [13] $a_\mu^{\rm exp} - a_\mu^{\rm th} = (25.2 \pm 9.2) \times 10^{-10}$, while that using the τ lepton data where applicable gives $a_\mu^{\rm exp} - a_\mu^{\rm th} = (9.4 \pm 10.5) \times 10^{-10}$. The experimental value $a_\mu^{\rm exp}$ is dominated by the BNL E821 measurement [14] $(11\ 659\ 208 \pm 5.8) \times 10^{-10}$. These differences correspond to 2.7 and 0.9 standard deviations, respectively, and thus there is a significant difference between the e^+e^--based and τ-based predictions. To clarify the situation, more data for $e^+e^- \to \pi^-\pi^+$ and for $\tau^- \to \pi^-\pi^0\nu_\tau$ decays are needed. In this paper we present a high-statistics measurement of the $\pi^-\pi^0$ mass spectrum produced in $\tau^-\to\pi^-\pi^0\,\nu_\tau$ decays [15] using data collected by the Belle experiment at the KEKB e^+e^- collider operating at a center-of-mass (CM) energy of 10.6 GeV. The data sample is about 50 times larger than those of previous experiments.

BASIC FORMULAE

The differential decay rate for $\tau^-\to\pi^-\pi^0\,\nu_\tau$ can be expressed as

$$\frac{1}{\Gamma}\frac{d\Gamma}{ds}(\tau^-\to\pi^-\pi^0\,\nu_\tau) = \frac{6\pi|V_{ud}|^2 S_{EW}}{m_\tau^2}\left(\frac{\mathcal{B}_e}{\mathcal{B}_{\pi\pi}}\right)\left(1-\frac{s}{m_\tau^2}\right)^2\left(1+\frac{2s}{m_\tau^2}\right)v_-(s), \qquad (1)$$

where s is the invariant-mass-squared of the $\pi^-\pi^0$ system, $v_-(s)$ is the vector spectral function characterizing the $\pi^-\pi^0$ system, $|V_{ud}|$ denotes the CKM mixing matrix element, and S_{EW} accounts for electroweak radiative corrections. $\mathcal{B}_e$ and $\mathcal{B}_{\pi\pi}$ are the branching fractions for $\tau^- \to e^-\nu_\tau\bar{\nu}_e$ and $\tau^-\to\pi^-\pi^0\,\nu_\tau$, respectively.

The corresponding $\pi^+\pi^-$spectral function $v_0(s)$ can be obtained from the $e^+e^- \to \pi^+\pi^-$ cross section:

$$\sigma(e^+e^- \to \pi^+\pi^-) = \frac{4\pi\alpha_0^2}{s}\,v_0(s), \qquad (2)$$

where s is the e^+e^- CM energy squared and α_0 is the fine-structure constant at $s = 0$. Up to isospin-violating effects, CVC allows one to relate the spectral function from τ decays to the isovector part of the e^+e^- spectral function [16]:

$$v_-(s) \;=\; v_0^{I=1}(s)\,. \tag{3}$$

The mass spectrum of the two-pion system is typically expressed in terms of pion form factors; these are useful for comparing resonance shapes in the charged and neutral two-pion systems. The spectral function $v_j(s)\,(j = -, 0)$ is related to the form factor $F_\pi^j(s)$ via

$$v_j(s) = \frac{\beta_j^3(s)}{12\pi}|F_\pi^j(s)|^2, \tag{4}$$

where $\beta_-(s)\,(\beta_0(s))$ is the pion velocity in the $\pi^-\pi^0$ $(\pi^+\pi^-)$ rest-system. The velocities $\beta_j(s)$ are explicitly given by $\beta_-^2(s) = [1-(m_{\pi^-}-m_{\pi^0})^2/s]\,[1-(m_{\pi^-}+m_{\pi^0})^2/s]$ and $\beta_0^2(s) = [1-4m_{\pi^-}^2/s]$.

The leading-order hadronic contribution to the muon anomalous magnetic moment $(a_\mu^{\rm had,LO})$ is related to the e^+e^- annihilation cross section via the dispersion integral

$$a_\mu^{\rm had,LO} \;=\; \left(\frac{\alpha_0 m_\mu}{3\pi}\right)^2 \int_{4m_\pi^2}^{\infty} \frac{R(s)}{s^2}\hat{K}(s)\,ds\,, \tag{5}$$

where s is the invariant-mass-squared of the two-pion system, and $R(s) = \sigma(e^+e^- \to \text{hadrons})/(4\pi\alpha_0^2/3s)$. The kernel $\hat{K}(s)$ is a smooth function increasing from 0.63 at the threshold $s = 4m_\pi^2$ to unity at $s{=}\infty$ [17]. Due to the $1/s^2$ dependence, hadronic final states at low energy dominate the contribution to $a_\mu^{\rm had,LO}$; in fact about 70% of $a_\mu^{\rm had,LO}$ is due to the two-pion state having $4m_\pi^2 \le s \le 0.8\ (\text{GeV}/c^2)^2$. Consequently, the 2π spectral function in τ data is useful to obtain predictions for $a_\mu^{\rm had,LO}$. Using Eqs. (2) and (3) to evaluate (5) we obtain

$$a_\mu^{\pi\pi} \;=\; \left(\frac{\alpha_0 m_\mu}{3\pi}\right)^2 \int_{4m_\pi^2}^{m_\tau^2} \frac{3\,v_-(s)}{s^2}\hat{K}(s)\,ds \,+\ldots\,, \tag{6}$$

where "..." indicates the integral above the m_τ^2 region. To determine $v_-(s)$, one must measure both the branching fraction for $\tau^-{\to}\,\pi^-\pi^0\,\nu_\tau$ and the $\pi^-\pi^0$ mass spectrum $(1/N)(dN/ds)$. Here we report new measurements for both of these.

DATA SAMPLE AND SELECTION CRITERIA

The data sample used was collected by the Belle detector at the KEKB energy-asymmetric e^+e^- collider [18]. It is based on an integrated luminosity of 72.2 fb^{-1} recorded at a CM energy of 10.6 GeV. The Belle detector is a large-solid-angle magnetic spectrometer consisting of a three-layer silicon-vertex detector (SVD), a 50-layer central drift chamber (CDC) for charged particle tracking and specific ionization measurement (dE/dx), an array of aerogel threshold Cerenkov counters (ACC), a barrel-like arrangement of time-of-flight scintillation counters (TOF), and an electromagnetic calorimeter (ECL) comprised of CsI(Tl) crystals located inside a superconducting solenoid coil that provides a 1.5 T magnetic field. An iron flux-return located outside of the coil is instrumented to identify muons and to detect K_L^0 mesons (KLM). The detector is described in detail elsewhere [19].

To study backgrounds and determine selection criteria, we perform Monte Carlo (MC) simulation studies for various processes. The KORALB/TAUOLA program [20, 21] is used for $\tau^+\tau^-$-pair generation, the QQ generator [22] for $\bar{B}B$ and $\bar{q}q$ continuum processes, the BHLUMI [23] program for radiative Bhabha events, the KKMC [24] program for radiative $\mu^+\mu^-$-pair events, and the AAFHB [25] program for two-photon processes. The BHLUMI and KKMC programs include higher-order radiative corrections and are among the most accurate programs available. The detector response is simulated by a GEANT-based program [26]. In order to realistically simulate beam-induced background, detector hits taken from randomly-triggered data are added to wire hits in the CDC and to energy deposits in the ECL.

$\tau^+\tau^-$ pair selection

The event selection consists of two steps. Initially, a sample of generic $e^+e^- \to \tau^+\tau^-(\gamma)$ events are selected with relatively loose criteria. From this sample $\tau^- \to \pi^-\pi^0\,\nu_\tau$ decays are then selected. The number of generic $\tau^+\tau^-$ events is used to determine the $\tau^- \to \pi^-\pi^0\,\nu_\tau$ branching fraction.

Generic $\tau^+\tau^-$ events are selected by requiring that the number of charged tracks in an event be two or four with zero net charge; that each track have a momentum transverse to the beam axis (p_T) of greater than 0.1 GeV/c; and that each track extrapolate to the interaction point (IP) within ± 1 cm transversely and within ± 5 cm along the beam direction. To suppress background from Bhabha and $\mu^+\mu^-$ events, the reconstructed CM energies and the sum of the momenta of the two leading tracks are required to be less than 9.0 GeV/c. The maximum p_T among the tracks is required to be greater than 0.5 GeV/c. Beam-related background is rejected by requiring that the position of the reconstructed event vertex be less than 0.5 cm from the IP in the transverse direction and less than 2.5 cm from the IP along the beam direction. The polar angle of the leading particle with respect to the beam axis (θ^*) in the CM frame is required to be in the fiducial region of the detector: $35^\circ < \theta^* < 145^\circ$.

To reduce remaining background from Bhabha, $\mu^+\mu^-\gamma$, and two-photon events, a cut is applied in the two-dimensional plane of the missing-mass MM and the direction of missing momentum in CM $\theta^*_{\rm miss}$, where MM is evaluated from the four-momenta of the measured tracks and photons: $(MM)^2 = (P_{\rm ini} - P_{\rm tracks} - P_{\gamma s})^2$. In this expression $P_{\rm ini}$ is the four-momentum of the initial e^+e^- system. Each photon (reconstructed from clusters in the calorimeter) must be separated from the nearest track projection by at least 20 cm and have an energy greater than 0.05 GeV in the central part ($-0.63 \le \cos\theta < 0.85$), and 0.1 GeV in the endcap part ($-0.90 \le \cos\theta < -0.62$ and $0.85 \le \cos\theta < 0.95$). Photons measured at the detector edge are rejected. A scatterplot of MM vs. $\theta_{\rm miss}$ for data is shown in Fig. 1. In this plot, events at $MM \approx 0$ are due to radiative Bhabha events and $e^+e^- \to \mu^+\mu^-(\gamma)$, while events in the high-MM region are from two-photon processes. Events within the octagonal region are selected as $\tau^+\tau^-$candidates.

Candidate events are divided into two hemispheres in the CM frame with respect to the highest momentum particle, and the remaining background from e^+e^- annihilation processes is suppressed by selecting events with low multiplicity as characterized by the quantity $X_{\rm part} \equiv (n_{\rm tr} + n_\gamma)_1 \times (n_{\rm tr} + n_\gamma)_2$, where $n_{{\rm tr},j}$ and $n_{\gamma,j}$ are the numbers of tracks and photons in hemisphere j. We require $X_{\rm part} \le 25$. Finally, in order to eliminate Bhabha events in which one or both electrons produce a shower in material near the interaction region, the

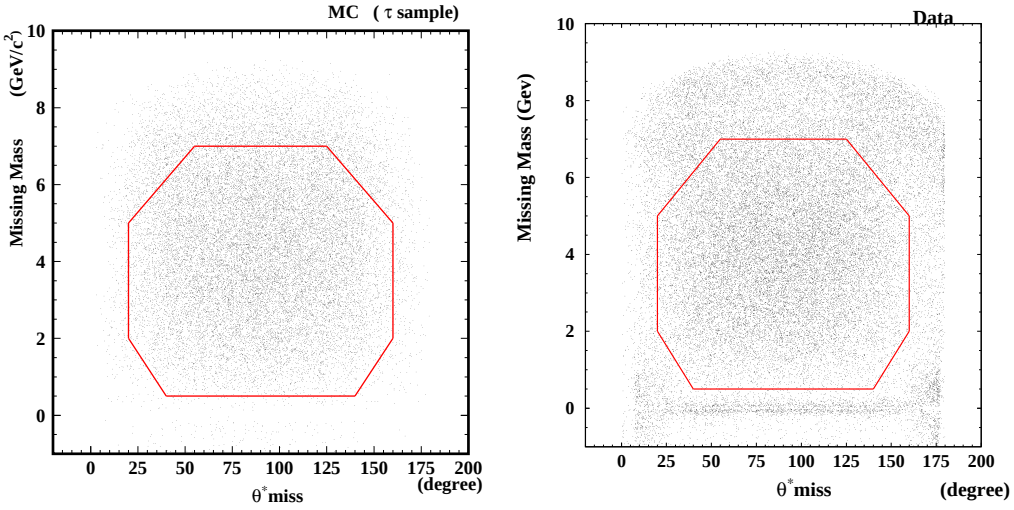

FIG. 1: Missing mass (MM) versus the polar angle for the direction of the missing momentum ($\theta^*_{\rm miss}$). The left plot shows MC $e^+e^- \to \tau^+\tau^-$ events, and the right plot shows the data. Events inside the octagonal region are selected as $\tau^+\tau^-$-pair candidates.

acoplanarity angle ξ between the first and second highest momentum tracks is required to be $\xi > 1^\circ$, where $\xi \equiv ||\phi_1 - \phi_2| - \pi|$ is defined as the two-track acollinearity in azimuth.

After applying all selection criteria, 22.71×10^6 $\tau^+\tau^-$-pairs survive. The background is estimated using MC simulation. The dominant source is from continuum processes $e^+e^- \to q\bar{q}\,(q = u, d, s, c)$ and amounts to 5.5%. Backgrounds from Bhabha events, $\mu^+\mu^-(\gamma)$, and two-photon $e^+e^- \to e^+e^-e^+e^-(\mu^+\mu^-)$ events are estimated to be 0.6%, 0.4%, and 0.8%, respectively. Other sources are found to be small. These background estimates are checked by comparing the number of events in control samples. The control samples for continuum, Bhabha + $\mu^+\mu^-$, and two-photon processes are high multiplicity events having $25 < X_{\rm part} < 30$ or $|MM| < 0.5$ GeV/c^2 or $|MM| > 8.0$ GeV/c^2, respectively. The differences in event yields for these control samples and the MC predictions (5-10%) are included as systematic errors for the results discussed in latter sections.

$\tau^- \to \pi^-\pi^0\,\nu_\tau$ candidate selection

Within the $\tau^+\tau^-$-pair sample, $\tau^- \to \pi^-\pi^0\,\nu_\tau$ decays are reconstructed by requiring that there be both one charged track and one π^0 in one hemisphere. The π^0 candidate is selected based on the normalized invariant mass $S_{\gamma\gamma} \equiv (m_{\gamma\gamma} - m_{\pi^0})/\sigma_{\gamma\gamma}$, where $\sigma_{\gamma\gamma}$ is the mass resolution of the $\gamma\gamma$ system. The value of $\sigma_{\gamma\gamma}$ ranges from 0.005 GeV to 0.008 GeV, depending on the π^0 momentum and polar angle. Pairs of photons with $|S_{\gamma\gamma}| < 9.0$ are considered as π^0 candidates. To keep beam-related background at a negligible level, we require that the CM momentum of the π^0 be greater than 0.25 GeV/c and the photon CM energy be greater than 0.08 GeV.

The distribution in the normalized di-photon invariant mass $S_{\gamma\gamma}$ for the selected $\pi^-\pi^0$ sample, where there are one charged track and one π^0 candidate in one hemisphere, is shown in Fig. 2. The lower-side tail of the $S_{\gamma\gamma}$ distribution is primarily due to rear and

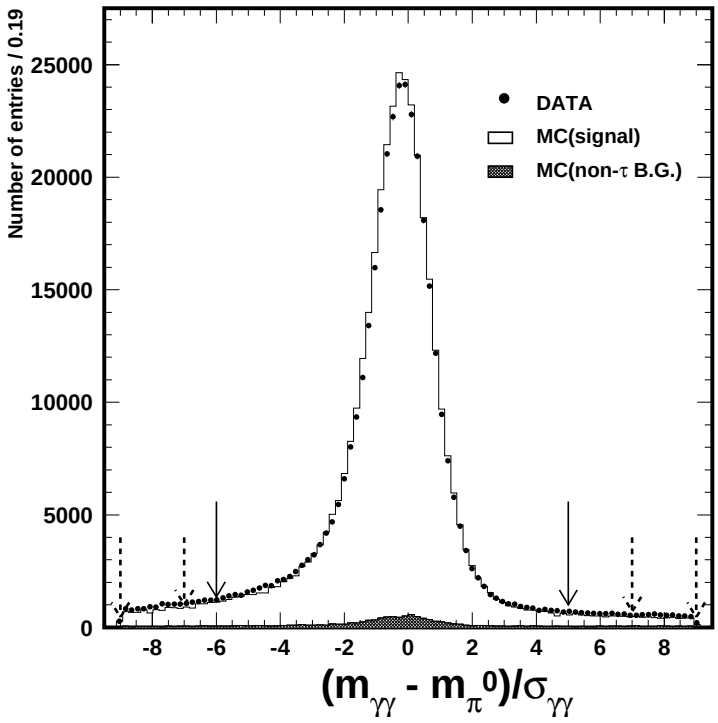

FIG. 2: Normalized $\gamma\gamma$ invariant mass ($S_{\gamma\gamma}$) spectrum in the data(points) and the $\tau^+\tau^-$ MC event(histogram), for the sample described in the text. The plotted data correspond to 6.1% of the full data used in this analysis. The arrows indicate the signal region $-6 < S_{\gamma\gamma} < 5$ and the sideband regions $9 < |S_{\gamma\gamma}| < 7$. The sideband regions are used to subtract fake-π^0 background.

transverse leakage of electromagnetic showers out of the CsI(Tl) crystals and the conversion of the photons in the material located in front of the crystals. Good agreement between data and Monte-Carlo indicates that these effects are properly modeled by the Monte-Carlo simulation. We define the interval $-6.0 < S_{\gamma\gamma} < 5.0$ as the π^0 signal region. Spurious π^0 background is small and estimated from the sideband regions $7 < |S_{\gamma\gamma}| < 9$. To reduce feed-down background from multi-π^0 decays such as $\tau^- \to \pi^-(n\pi^0)\nu_\tau$ ($n \geq 2$), signal candidates (in a hemisphere) are rejected if there are additional γ's in the same hemisphere with energy greater than 0.2 GeV.

The $\pi^-\pi^0$ invariant-mass-squared ($M^2_{\pi\pi^0}$) spectrum is obtained assuming the pion mass for the charged track; it is shown in Fig. 3 along with the MC prediction. To improve the energy resolution of the π^0, a π^0 mass constraint is imposed. The amount of a spurious π^0 background depends on the $M^2_{\pi\pi^0}$ region, varying from 4% to 15%. (This is subtracted using $S_{\gamma\gamma}$ sidebands.) The final sample contains 5.55×10^6 $\tau^- \to h^-\pi^0\,\nu_\tau$ candidates after the π^0 background subtraction, where h^- denotes π or K. This sample is 50 times larger than those of previous studies.

Feed-down background arises mainly from multi-π^0 modes such as $\tau^- \to \pi^-(n\pi^0)\nu_\tau$ (5.5%) and $\tau \to K^-\pi^0\nu_\tau$ (0.48%). Including other modes, the total feed-down background is (6.0 ± 0.1)%. The error listed includes statistical uncertainty as well as the uncertainty in relevant branching fractions. Background from non-τ processes is negligible, except that from continuum processes. The amount of continuum background is estimated from MC

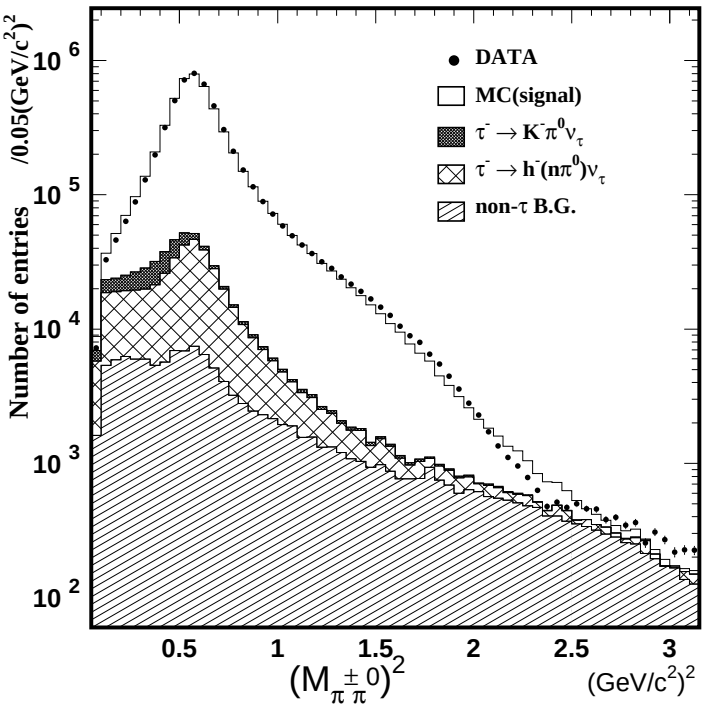

FIG. 3: Invariant-mass-squared ($M^2_{\pi\pi^0}$) distribution for $\tau^-\to\pi^-\pi^0\,\nu_\tau$. The solid circles with error bars represent the data, and the histogram represents MC simulation (signal + background). The open area shows the contribution from $\tau^-\to\pi^-\pi^0\,\nu_\tau$; the narrow cross-hatched area shows that from $\tau^-\to K^-\pi^0\nu_\tau$; the wide cross-hatched area shows that from $\tau^-\to h^-(n\pi^0)\nu_\tau$; and the striped area shows that from $q\bar{q}$ continuum and other non-τ processes.

simulation to be $(2.45\pm0.05)\%$. The normalization of the continuum MC is checked using data in the high-mass region $M^2_{\pi\pi^0} > M^2_\tau$.

The MC simulation of τ decays is based on the TAUOLA program [21]. A small difference observed between data and MC in Fig.3 for $M^2_{\pi\pi^0} \geq 2.0$ $(\mathrm{GeV/c^2})^2$ is attributed to the $\rho''(1700)$ resonance, which is not included in the current TAUOLA program.

MEASUREMENT OF THE BRANCHING FRACTION

Formula

The branching fraction for $\tau^-\to h^-\pi^0\,\nu_\tau$ ($\mathcal{B}_{h\pi^0}$) is determined by dividing the signal yield $N_{h\pi^0}$ by the number of selected generic $\tau^+\tau^-$-pairs $N_{\tau\tau}$:

$$\mathcal{B}_{h\pi^0} \;=\; \frac{N_{h\pi^0}}{2N_{\tau\tau}}\cdot\frac{(1-b^{\text{feed-down}}-b^{\text{non-}\tau})}{(1-b_{\tau\tau})}\cdot\left(\frac{\epsilon_{\tau\tau}}{\epsilon^{\tau}_{h\pi^0}}\right)\cdot\frac{1}{\epsilon^{ID}_{h\pi^0}}\,. \tag{7}$$

In this formula, $b_{\tau\tau}$ is the background fraction in the $\tau^+\tau^-$ sample, $\epsilon_{\tau\tau}$ is the efficiency of the $\tau^+\tau^-$-pair selection, $\epsilon^{\tau}_{h\pi^0}$ is the efficiency for $\tau^-\to h^-\pi^0\nu$ decays to pass the $\tau^+\tau^-$-pair selection, and $\epsilon^{ID}_{h\pi^0}$ is the efficiency for $\tau^-\to h^-\pi^0\nu$ decays satisfying the $\tau^+\tau^-$-pair selection

to pass the $h^-\pi^0$ selection. The product $\epsilon^{\tau}_{h\pi^0} \cdot \epsilon^{ID}_{h\pi^0}$ is the overall detection efficiency for the $h^-\pi^0\nu$ final state. The parameter $b^{\text{feed-down}}$ is the fraction of $h^-\pi^0\nu$ candidates coming from other τ decay modes, and $b^{\text{non-}\tau}$ is the fraction coming from non-τ processes. In this formula, several common uncertainties such as that in the luminosity, that in the cross section for $\tau^+\tau^-$-pair production, that in the trigger efficiency, and that in the $\tau^+\tau^-$ selection efficiency cancel in the ratio. The value for each factor is listed in Table I along with the statistical error.

Parameter	Values
$\varepsilon_{\tau\tau}$	30.81 ± 0.05 %
$\varepsilon^{\tau}_{h\pi^0}$	34.26 ± 0.07 %
$f_b = \dfrac{\varepsilon^{\tau}_{h\pi^0}}{\varepsilon_{\tau\tau}}$	1.112 ± 0.003
$\varepsilon^{ID}_{h\pi^0}$	42.62 ± 0.13 %
$b_{\tau\tau}$	7.66 ± 0.03 %
$b^{\text{feed-down}}_{h\pi^0}$	5.98 ± 0.08 %
$b^{\text{non-}\tau}_{h\pi^0}$	2.45 ± 0.06 %

TABLE I: Values of parameters used for the branching fraction measurement along with statistical errors.

Systematic uncertainty

The sources of systematic uncertainty are listed in Table II. The uncertainty in the tracking efficiency is estimated using $D^{*+} \to D^0\pi^+ \to K^-\pi^+\pi^+$ decays to be 1% per track. A large part of this uncertainty cancels in the ratio of Eq.(7); the resulting uncertainty from this source is $\Delta\mathcal{B}_{h\pi^0} = 0.12$ %. The γ/π^0 detection efficiency is obtained from the ratio of $D^0 \to K^-\pi^+\pi^0$ to $D^0 \to K^-\pi^+$ decays, in which the branching fractions are known precisely. The uncertainty is estimated to be $\pm 1.7\%$ for a π^0 momentum less than 1.0 GeV/c. As a consistency check, the branching fraction is re-measured after changing the photon threshold from 0.05 GeV to 0.10 GeV; the difference in $\mathcal{B}_{h\pi^0}$ is only 0.10%. The uncertainty in background in the non-τ sample $\delta b^{\text{non}-\tau}_{h\pi^0}$ is estimated from the control sample above the τ mass region, while the uncertainty in feed-down background $\delta b^{\text{feed}-\text{down}}_{h\pi^0}$ is obtained from the uncertainty in $\tau^- \to h^-(n\pi^0)\nu_\tau$ and $\tau^- \to K^-\pi^0\nu_\tau$ branching fractions.

The veto of additional γ's is required in the event selection to reduce background from multi-π^0 decay channels. However, it also vetoes signal if there are photons radiated in the initial or final state. In addition, photon candidates can also appear due to electromagnetic shower fragments and/or mis-reconstructed of electrons. The uncertainty from these sources is estimated by changing the veto threshold by ± 0.1 GeV; the resulting change in $\mathcal{B}_{h\pi^0}$ is only $\pm 0.05\%$. Signal events are flagged by several trigger conditions that require two or more CDC tracks with associated TOF hits, ECL clusters, or a significant sum of energy in the ECL. This redundancy allows one to monitor the efficiency of each trigger requirement. The

Source of uncertainty	$\Delta\mathcal{B}_{h\pi^0}$ (%)
Tracking efficiency	0.12
π^0/γ efficiency	0.25
Background for $\tau^+\tau^-$	0.09
Feed-down background for $\tau^-\to h^-\pi^0\,\nu_\tau$	0.04
Non-τ background for $\tau^-\to h^-\pi^0\,\nu_\tau$	0.05
γ veto	0.05
Trigger	0.08
MC statistics	0.04
Total	0.31

TABLE II: Systematic uncertainties for the $\tau^-\to h^-\pi^0\,\nu_\tau$ branching fraction.

uncertainty arising from the trigger is estimated by assuming there is a $\pm 3\%$ uncertainty in the track and energy trigger efficiencies, which is the maximum variation measured during experimental running. The resulting uncertainty on $\mathcal{B}_{h\pi^0}$ is small (0.08%) since the $\tau^+\tau^-$ trigger efficiency is high (97%).

Results

Inserting all values into Eq. (7) gives

$$\mathcal{B}_{h\pi^0} \;=\; (25.60 \,\pm\, 0.04 \,\pm\, 0.31)\%\,, \tag{8}$$

where the first error is statistical and the second is systematic. Subtracting the small kaon-channel branching fraction listed in the PDG [27] [$\mathcal{B}_{K^-\pi^0} = (0.45 \pm 0.03)\%$] gives a $\tau^-\to\pi^-\pi^0\,\nu_\tau$ branching fraction of

$$\mathcal{B}_{\pi\pi^0} \;=\; (25.15 \,\pm\, 0.04 \,\pm\, 0.31)\%\,. \tag{9}$$

This result is in good agreement with previous measurements, as shown in Table III. Our statistical error is significantly lower than those of the other measurements, while our systematic error is similar to those of the others (except for the ALEPH result).

Experiment	$\mathcal{B}_{h\pi^0}(\%)$	Reference
OPAL	$25.89 \pm 0.17 \pm 0.29$	[28]
ALEPH	$25.924 \pm 0.097 \pm 0.085$	[29]
L3	$25.05 \pm 0.35 \pm 0.50$	[30]
CLEO	$25.87 \pm 0.12 \pm 0.42$	[31]
This work	$25.60 \pm 0.04 \pm 0.31$	

TABLE III: Branching fractions for $\tau^-\to h^-\pi^0\,\nu_\tau$ measured by various experiments.

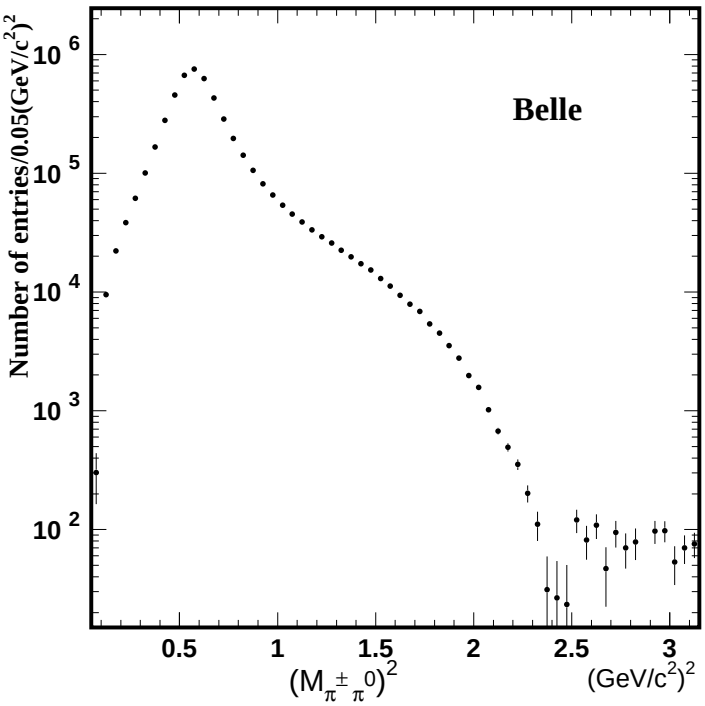

FIG. 4: Invariant-mass-squared ($M^2_{\pi\pi^0}$) distribution for $\tau^-\to\pi^-\pi^0\,\nu_\tau$ after background subtraction.

MEASUREMENT OF THE MASS SPECTRUM

In order to obtain the true $\pi^-\pi^0$ mass spectrum, one must correct for (1) background, (2) smearing due to finite resolution and radiative effects, and (3) mass-dependent acceptance.

Background Correction

As noted earlier, background entering the $\tau^-\to\pi^-\pi^0\,\nu_\tau$ sample is small. The sidebands of the $M_{\gamma\gamma}$ distribution are used to estimate the fake π^0 contribution. This background dominates at values of $M^2_{\pi\pi^0}$ less than about 0.25 $(\mathrm{GeV}/c^2)^2$.

As seen in Fig. 3, feed-down background arises from $\tau^-\to h^-(n\pi^0)\nu_\tau$ and $\tau^-\to K^-\pi^0\nu_\tau$ decays; both backgrounds dominate at low values of $M^2_{\pi\pi^0}$. In the high mass region, continuum background dominates. For this analysis we did not use information from particle identification (PID) detectors to separate charged pions from kaons, as the feed-down background is dominated by $\tau^-\to h^-(n\pi^0)\nu_\tau$ rather than $\tau^-\to K^-\pi^0\nu_\tau$. The $M^2_{\pi\pi^0}$ distribution after subtracting this background is shown in Fig. 4.

Acceptance Corrections

The detector effects include $M^2_{\pi\pi^0}$-dependent acceptance and bin-by-bin migration caused by the finite mass resolution. We correct for these effects by performing an unfolding proce-

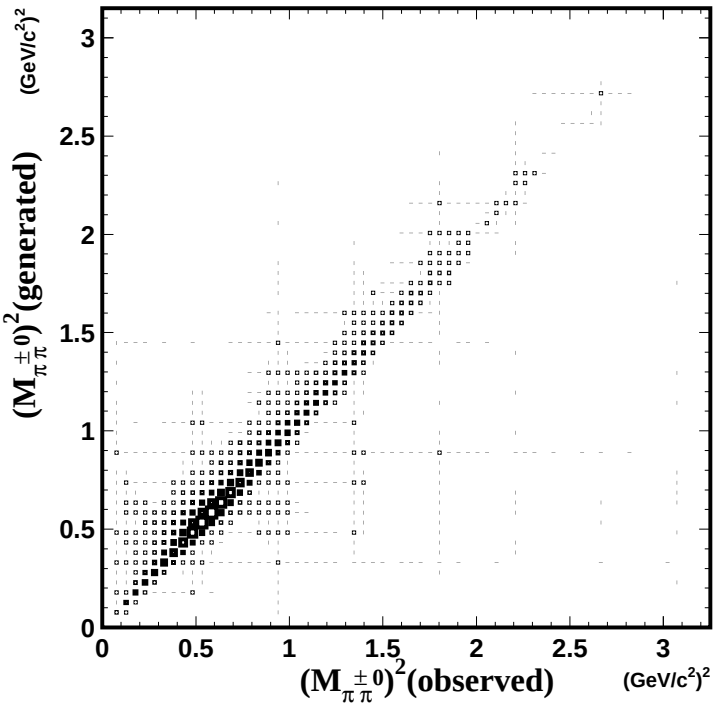

FIG. 5: Correlation between $M^2_{\rm gen}$ (vertical axis) and $M^2_{\rm obs}$ (horizontal axis), the generated and observed invariant masses squared of the $\pi^-\pi^0$ system in $\tau^-\to\pi^-\pi^0\,\nu_\tau$ decay.

dure. The unfolding program used is that employed by the ALEPH experiment [32]. In this program, the unfolding is based on the Singular-Value-Decomposition (SVD) method [32], in which the acceptance matrix is inverted by limiting the number of singular values to only those that are statistically significant. The output of the program is the unfolded distribution and its covariance matrix.

The correlation between the generated quantity $M^2_{\rm gen}$ and the measured one $M^2_{\rm obs}$ is shown in Fig. 5. The figure shows a clear correlation between $M^2_{\rm gen}$ and $M^2_{\rm obs}$. The resolution in $M^2_{\pi\pi^0}$ is 0.005 $({\rm GeV}/c^2)^2$ in the low-mass region and 0.030 $({\rm GeV}/c^2)^2$ in the high-mass region; thus the bin size chosen is $\Delta M^2 = 0.050$ $({\rm GeV}/c^2)^2$ so that the off-diagonal components of the acceptance matrix are small.

The acceptance as a function of $M^2_{\rm gen}$ is shown in Fig. 6. The acceptance varies smoothly and its average value is 17%. It decreases at low values of $M^2_{\rm gen}$ due to the overlap of γ clusters with the π^- track projection at the calorimeter.

Results

The unfolded $s = M^2_{(\pi\pi^0\,\rm unf.)}$ spectrum dN/ds is shown in Fig. 7. The square roots of the diagonal components of the covariance matrix are used as the errors. The ρ peak and the shoulder due to the $\rho'(1450)$ are clearly visible. The dip at $s \approx 2.5$ $({\rm GeV}/c^2)^2$ is caused by destructive interference between the $\rho'(1450)$ and $\rho''(1700)$ resonances.

To obtain parameters for the ρ, ρ' and ρ'' resonances, a χ^2 fit using Breit-Wigner functions

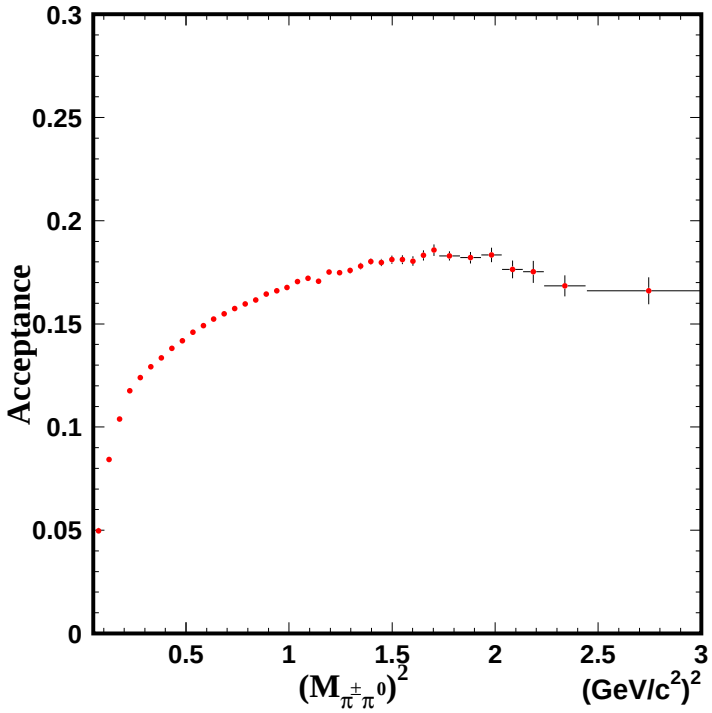

FIG. 6: Acceptance as a function of $M^2_{\rm gen}$, as determined from $\tau^-\to\pi^-\pi^0\,\nu_\tau$ MC simulation.

is performed. Since the unfolded mass spectrum has bin-by-bin correlations, the off-diagonal components of the covariance matrix X are included in the χ^2 evaluation:

$$\chi^2 = \sum_{i,j} \left(y_i - f(s_i;\alpha)\right) \left(X^{-1}\right)_{ij} \left(y_j - f(s_j;\alpha)\right) \,, \tag{10}$$

where y_i is the measured value at the i-th bin, $f(s;\alpha)$ is the value of the function for parameters α, and $(X^{-1})_{ij}$ is the inverse of the covariance matrix.

In the fit, the s dependence of the decay rate is given by Eq. (1). The pion form factor in Eq. (4) is parametrized with Breit-Wigner functions corresponding to the ρ, $\rho'(1450)$, and $\rho''(1700)$ resonances:

$$F_\pi(s) = \frac{1}{1+\beta+\gamma}(BW_\rho + \beta\cdot BW_{\rho'} + \gamma\cdot BW_{\rho''}) \,, \tag{11}$$

where the parameters β and γ (denoting the relative size of the two resonances) are in general complex. We use the Gounaris-Sakurai (GS) model [33] for the Breit-Wigner shape:

$$BW_i^{GS} = \frac{M_i^2 + d\cdot M_i\Gamma_i(s)}{(M_i^2 - s) + f(s) - i\sqrt{s}\Gamma_i(s)} \,, \tag{12}$$

with an energy-dependent width

$$\Gamma_i(s) = \Gamma_i \left(\frac{M_i^2}{s}\right)\left(\frac{k(s)}{k(M_i^2)}\right)^3 \,. \tag{13}$$

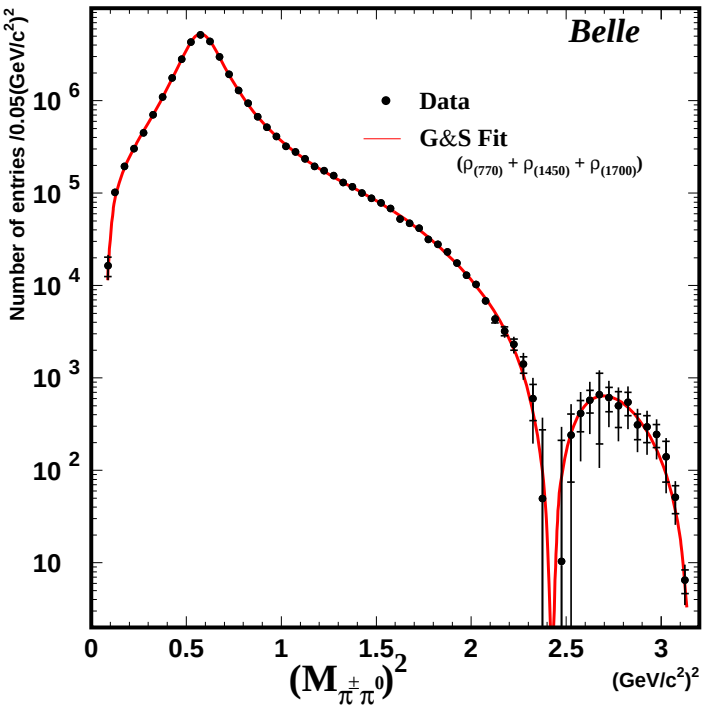

FIG. 7: Fully-corrected $M^2_{\pi\pi^0}$ distribution for $\tau^-\to\pi^-\pi^0\,\nu_\tau$. The solid curve is the result of a fit to the Gounaris-Sakurai model with $\rho(770)$, $\rho'(1450)$, and $\rho''(1700)$ resonances. All parameters are floated.

Here, $k(s)=\frac{1}{2}\sqrt{s}\beta_-(s)$ is the pion momentum in the $\pi^-\pi^0$ rest frame. The functions $f(s)$ and $h(s)$ are defined as

$$f(s) \;=\; \Gamma_i\,\frac{M_i^2}{k^3(M_i^2)}\left[k^2(s)\left(h(s)-h(M_i^2)\right)+(M_i^2-s)k^2(M_i^2)\left.\frac{dh}{ds}\right|_{s=M_i^2}\right] \tag{14}$$

$$h(s) \;=\; \frac{2}{\pi}\frac{k(s)}{\sqrt{s}}ln\frac{\sqrt{s}+2k(s)}{2m_\pi}\,, \tag{15}$$

with $dh/ds|_{M_i^2}=h(M_i^2)\left[(8k^2(M_i^2))^{-1}-(2M_i^2)^{-1}\right]+(2\pi M_i^2)^{-1}$ and

$$d=\frac{3}{\pi}\frac{m_\pi^2}{k^2(M_i^2)}ln\frac{M_i+2k(M_i^2)}{2m_\pi}+\frac{M_i}{2\pi k(M_i^2)}-\frac{m_\pi^2 M_i}{\pi k^3(M_i^2)}\,. \tag{16}$$

There are ten parameters in this formula: the masses (M_i) and the widths (Γ_i) for the ρ, ρ', and ρ'' resonances, their relative amplitudes $|\beta|,|\gamma|$, and their phases ϕ_β and ϕ_γ.

All parameters are floated in the fit. When evaluating the χ^2, the 1% systematic uncertainty resulting from the unfolding procedure is included in the diagonal part of the covariance matrix. This uncertainty is estimated by applying the same unfolding procedure to MC events and comparing the unfolded spectrum with the original. The result of the fit is shown in Fig. 7 as the solid line; the values obtained for the parameters are listed in

Parameter	Fit result (all free)	Fit result (fixed ϕ_γ)
M_ρ (MeV/c^2)	$774.6 \pm 0.2 \pm 0.3$	$774.3 \pm 0.2 \pm 0.3$
Γ_ρ (MeV)	$150.6 \pm 0.3 \pm 0.5$	$150.0 \pm 0.3 \pm 0.5$
$M_{\rho'}$ (MeV/c^2)	$1336 \pm 12 \pm 23$	$1436 \pm 15 \pm 23$
$\Gamma_{\rho'}$ (MeV)	$471 \pm 29 \pm 21$	$553 \pm 31 \pm 21$
$\lvert\beta\rvert$	$0.090 \pm 0.009 \pm 0.013$	$0.161 \pm 0.020 \pm 0.013$
ϕ_β (degree)	$123.7 \pm 5.0 \pm 7.0$	$149.1 \pm 2.4 \pm 7.0$
$M_{\rho''}$ (MeV/c^2)	$1600 \pm 13 \pm 4$	$1804 \pm 16 \pm 4$
$\Gamma_{\rho''}$ (MeV)	$255 \pm 19 \pm 79$	$567 \pm 81 \pm 79$
$\lvert\gamma\rvert$	$0.062 \pm 0.015 \pm 0.015$	$0.136 \pm 0.024 \pm 0.015$
ϕ_γ (degree)	-64.1 ± 7.9	[0]
χ^2/d.o.f	55/51	94/52

TABLE IV: Results of fitting the $M^2_{\pi\pi^0}$ distribution for $\tau^- \to \pi^-\pi^0\,\nu_\tau$ to the Gounaris-Sakurai model with the $\rho(770)$, $\rho'(1450)$, and $\rho''(1700)$ resonances. The results for two cases, all parameters floated (the second column) and fixed ϕ_γ (the third column) are shown. For both cases, the first error is statistical and the second one is systematic. The systematic errors include the uncertainty of the backgrounds, unfolding, as well as the uncertainty of the photon energy scale.

Table IV. The results are compared with the previous ALEPH measurements in Table V. In the table, the first error is statistical and the second one is systematic.

The main sources of systematic uncertainty are the photon energy scale, the unfolding procedure, and the background subtraction. The uncertainty in the ρ mass (0.3 MeV) is mainly due to the uncertainty in the photon energy scale. The uncertainty in background dominates for the ρ'' parameters. Our result for the mass of the ρ resonance agrees well with the ALEPH [29] and CLEO[11] results.

As can be seen from the second and third columns of Table V, where the interference angle ϕ_γ or three parameters $M_{\rho''}, \Gamma_{\rho''}, \phi_\gamma$ are fixed, respectively, as in the previous ALEPH [29] fit, the values for ρ' and ρ'' resonance parameters are quite sensitive to the values of other parameters fixed in the fit.

The results are shown in terms of the pion form factor squared ($|F_\pi(s)|^2$) in Figs. 8 and 9. A dip caused by destructive interference between the $\rho'(1450)$ and $\rho''(1700)$ is clearly visible. For the first time production of the $\rho''(1700)$ in τ^- decays has been unambiguously demonstrated and its parameters determined. For comparison, the figures also show results from the CLEO [11] and ALEPH [29] experiments, respectively; there is good agreement with both data sets. Figure 10 shows our data and that of CLEO for the mass range 0.2–2.2 GeV/c^2, where the contribution to $a_\mu^{\rm had,LO}$ is largest.

Parameter	This work (fixed ϕ_γ)	This work (fixed $M_{\rho''}, \Gamma_{\rho''}, \phi_\gamma$)	ALEPH(τ)
M_{ρ^-} (MeV/c^2)	774.3 $\pm$ 0.2	773.9 $\pm$ 0.1	775.5 $\pm$ 0.7
Γ_{ρ^-} (MeV)	150.0 $\pm$ 0.3	150.8 $\pm$ 0.3	149.0 $\pm$ 1.2
$M_{\rho'}$ (MeV/c^2)	1436 $\pm$ 15	1395 $\pm$ 4	1328 $\pm$ 15
$\Gamma_{\rho'}$ (MeV)	553 $\pm$ 31	411 $\pm$ 9	468 $\pm$ 41
$\lvert\beta\rvert$	0.161 $\pm$ 0.020	0.095 $\pm$ 0.02	0.120 $\pm$ 0.008
ϕ_β (degree)	149.1 $\pm$ 2.4	161 $\pm$ 2.0	153 $\pm$ 7
$M_{\rho''}$ (MeV/c^2)	1804 $\pm$ 16	[1713]	[1713]
$\Gamma_{\rho''}$ (MeV)	567 $\pm$ 81	[235]	[235]
$\lvert\gamma\rvert$	0.136 $\pm$ 0.024	0.045 $\pm$ 0.002	0.023 $\pm$ 0.008
ϕ_γ (degree)	[0]	[0]	[0]
χ^2/(d.o.f)	94 / 52	134/54	119 / 110
Reference			[29]

TABLE V: Comparison of our fit results for the $\rho(770)$, $\rho'(1450)$, and $\rho''(1700)$ parameters with those obtained by the ALEPH experiment[29]. The numbers in brackets indicate the values fixed in the fit.

EVALUATION OF $a_\mu^{\pi\pi}$

Using the unfolded $s = M^2_{(\pi\pi^0\,\mathrm{unf.})}$ distribution $(1/N)(dN/ds)$, the spectral function v^- is obtained by taking the inverse of Eq. (1):

$$v_- \;=\; \frac{m_\tau^2}{6\pi|V_{ud}|^2 S_{EW}} \left(\frac{\mathcal{B}_{\pi\pi}}{\mathcal{B}_e}\right) \left[\left(1-\frac{s}{m_\tau^2}\right)^2 \left(1+\frac{2s}{m_\tau^2}\right)\right]^{-1} \frac{1}{N}\frac{dN}{ds}\,. \tag{17}$$

The resulting function can be inserted into Eq. (6) to obtain the dominant low-mass contribution to the hadronic part of the anomalous magnetic moment, $a_\mu^{\pi\pi}$. This assumes the CVC relation (3) holds.

There are several external parameters in these equations; the values used for these are listed in Table VI. For m_τ, V_{ud}, and $\mathcal{B}_e$, PDG [27] values are used. For the electroweak radiative correction S_{EW}, we use the recent value 1.0233 ± 0.0006, which is based on a consistent treatment of the isospin-breaking correction [2, 34]. For the $\pi^-\pi^0$ branching fraction, our measurement is consistent with the world average given in Ref. [10].

Including our result and the recent ALEPH $\mathcal{B}_{\pi\pi^0}$ measurement, the new world average is

$$\mathcal{B}_{\pi\pi^0} = (25.42 \pm 0.11)\%. \tag{18}$$

We use this new world average for the evaluation of $a_\mu^{\pi\pi}$.

The integration in Eq. (6) is carried out numerically by taking the sum of the integrand evaluated at the center of each bin. The statistical error in $a_\mu^{\pi\pi}$ is calculated including the off-diagonal elements of the covariance matrix X_{ij}:

$$\delta a_\mu^{\pi\pi} \;=\; \sum_{i,j} \left(\frac{\partial a_\mu}{\partial \alpha_i}\right) X_{ij} \left(\frac{\partial a_\mu}{\partial \alpha_j}\right). \tag{19}$$

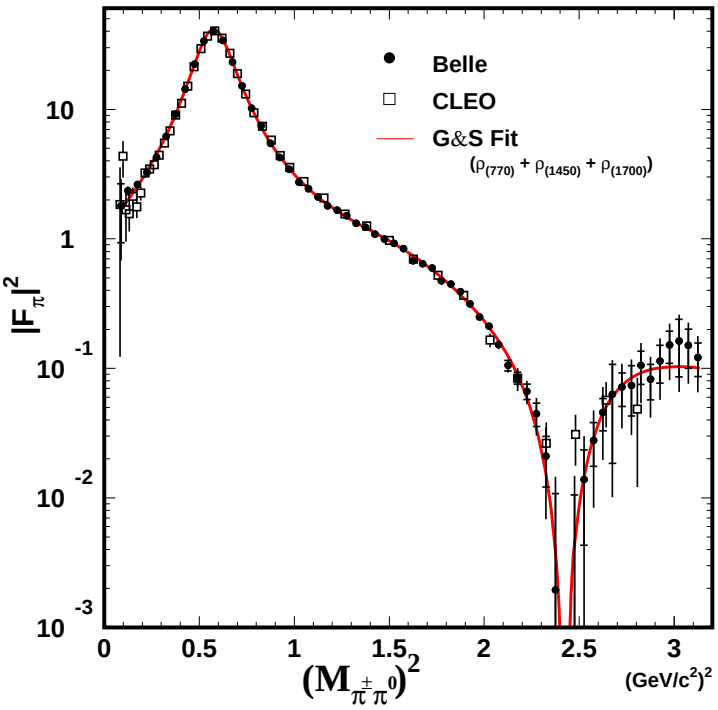

FIG. 8: Pion form factor for $\tau^- \to \pi^- \pi^0 \nu_\tau$. The solid circles show the Belle result and the open squares show the CLEO result [11]. The error bars for the Belle data include both statistical and systematic errors added in quadrature. The solid curve is the result of a fit to the Gounaris-Sakurai model with the $\rho(770)$, $\rho'(1450)$, and $\rho''(1700)$ resonances, where all parameters are floated.

Source	Value	Relative error (%)	$\Delta a_\mu^{\pi\pi}$ (10^{-10})	Reference
S_{EW}	1.0233 ± 0.0006	0.06	$\pm$ 0.32	[2],[34]
V_{ud}	0.9734 ± 0.0008	0.08	$\pm$ 0.42	[27]
$\mathcal{B}_e$	$(17.84 \pm 0.06)\%$	0.34	$\pm$ 1.82	[27]
$\mathcal{B}_{\pi\pi^0}$	$(25.42 \pm 0.11)\%$	0.43	$\pm$ 2.30	
Total external			$\pm$ 3.0	

TABLE VI: Values of the external parameters and the systematic errors for $a_\mu^{\pi\pi}$ arising from these sources.

Because of uncertainties associated with the background estimate and with the acceptance correction in the lowest mass region, the integration is carried out over the mass range $\sqrt{s} = 0.50$–1.80 GeV/c^2.

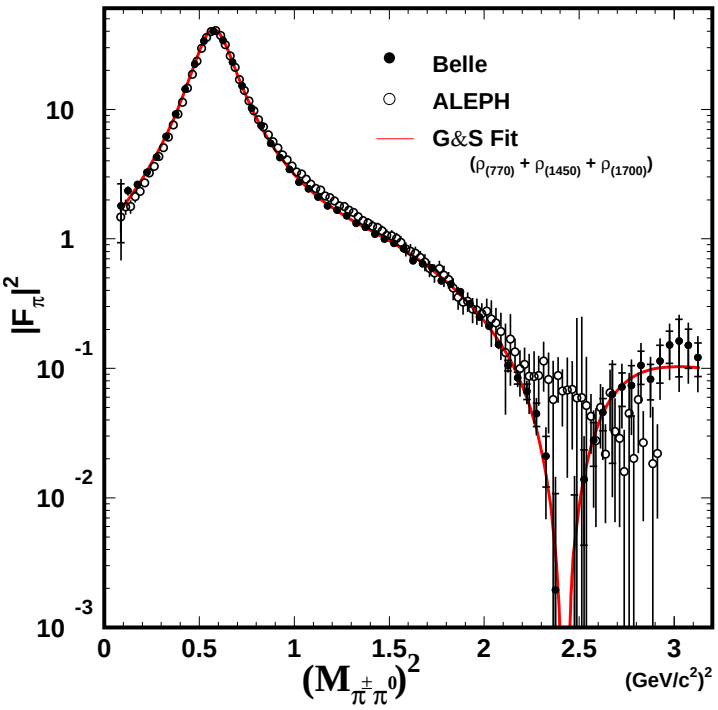

FIG. 9: Pion form factor for $\tau^- \to \pi^-\pi^0\,\nu_\tau$. The solid circles show the Belle result and the open squares show the ALEPH result [29]. The error bars for the Belle data include both statistical and systematic errors added in quadrature. The solid curve is the result of a fit to the Gounaris-Sakurai model, where all parameters are floated.

Systematic uncertainty

Systematic uncertainty in $a_\mu^{\pi\pi}$ arises from both external and internal sources. The errors arising from external parameters are summarized in Table VI; the total systematic error from these sources is $\pm 3.0 \times 10^{-10}$ (dominated by $\delta\mathcal{B}_{\pi\pi^0}$).

The systematic error arising from internal sources (specific to this measurement) are listed in Table VII. There are two sources of background in the $\pi^-\pi^0$ sample: (i) feed-down from $\tau^- \to h^-(n\pi^0)\nu_\tau$ and $\tau^- \to K^-\pi^0\nu_\tau$, and (ii) non-$\tau$ background. In the first case, the uncertainty in the branching fraction is used to estimate the error. In the second case, the uncertainty in the background as estimated from the control samples is assigned as the error. As mentioned earlier, the fake-π^0 background is subtracted using sideband events; the uncertainty is determined by varying the signal and sideband regions.

The ratio of the branching fractions for the decays $D^0 \to K^-\pi^-\pi^0$ and $D^0 \to K^-\pi^+$ is used to monitor the π^0 efficiency. It is found that the shape of the mass spectrum is insensitive to uncertainty in the π^0 efficiency, as it is only at the few % level. Adding all individual errors in quadrature gives a total error on $a_\mu^{\pi\pi}$ arising from internal sources of $\pm 1.0 \times 10^{-10}$.

To check the stability of $a_\mu^{\pi\pi}$, we perform the following tests:

1. The sample is divided into subsamples based on the tag-side topology, i.e., one electron,

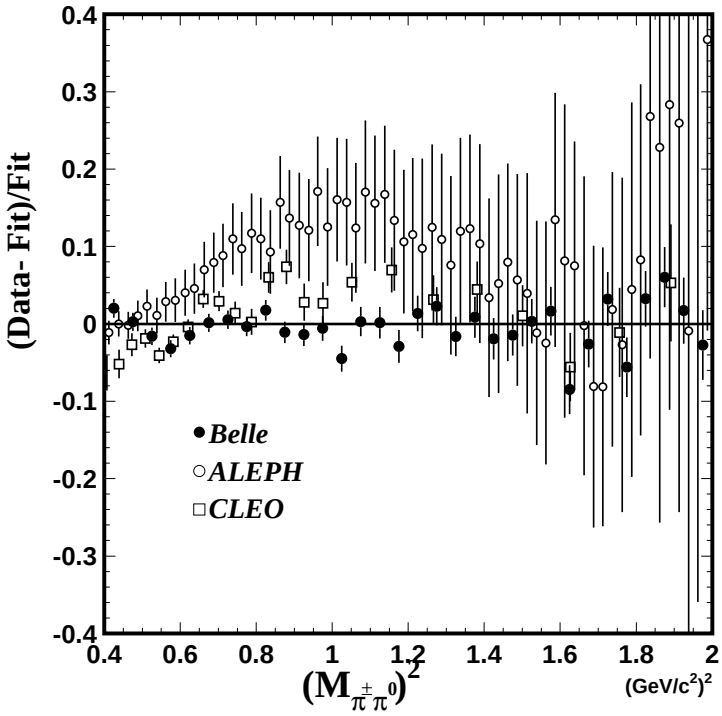

FIG. 10: Comparison of the pion form factor squared $|F_\pi(s)|^2$ measured by Belle to that measured by CLEO [11] and ALEPH [29] experiments in the $\rho(770)$ and $\rho'(1430)$ mass region. Difference from the fit of the Belle $\tau^-\to\pi^-\pi^0\,\nu_\tau$ data divided by the fit value is plotted.

one-prong, or three-prong. The values of $a_\mu^{\pi\pi}$ obtained from these subsamples are consistent within the statistical errors.

2. The sample is divided into subsamples based on the running period, e.g., years 2000, 2001, or 2002. Again, the values of $a_\mu^{\pi\pi}$ obtained are consistent within the statistical errors.

3. The sample might be sensitive to the requirement on the overlap region between the projection of the charged track and γ clusters. To estimate this sensitivity, we select events with a tighter isolation requirement on γ's and on the track extrapolation: 50 cm instead of 20 cm.

   The resulting variation in $a_\mu^{\pi\pi}$ is small and is included as an additional systematic error.

RESULTS

The result for $a_\mu^{\pi\pi}$ integrated over the mass range $\sqrt{s}$ =0.50–1.80 GeV/c^2 is

$$a_\mu^{\pi\pi}[0.50, 1.80] = (464.4 \pm 0.6\,(\text{stat.}) \pm 1.0\,(\text{sys.}) \pm 3.0\,(\text{sys. ext.}) \times 10^{-10},$$

where the first error is statistical and the second and third errors are systematic errors arising from internal and external sources, respectively. In addition, there is a systematic

Source	$\Delta a_\mu^{\pi\pi} \times 10^{10}$ (0.50–1.80 GeV/c^2)
Background:	
non-τ ($e^+e^- \to \bar{q}q$)	± 0.11
feed-down $h(n\pi^0)\nu$	± 0.09
feed-down $K^-\pi^0\nu$	± 0.15
Energy scale	± 0.10
π^0/γ selection	± 0.24
γ veto	± 0.93
Efficiency:	
π^0/γ	± 0.35
charged track	< 0.10
Integration procedure	< 0.10
Total internal	$\pm$ 1.04

TABLE VII: Systematic errors for $a_\mu^{\pi\pi}$ arising from internal sources (specific to this measurement).

uncertainty caused by isospin violation effects arising from ρ-ω interference, from the π^- and π^0 mass difference, and from radiative corrections (see Ref. [34]). The overall correction is estimated to be $(-1.8 \pm 2.3) \times 10^{-10}$, where the central value is taken from Ref. [11] and we enlarged the error according to the value in Table 5 of Ref. [2]; this correction is small because the threshold region is not included. Applying this correction gives

$$a_\mu^{\pi\pi}[0.50, 1.80] = (462.6 \pm 0.6\,(\text{stat.}) \pm 3.2\,(\text{sys.}) \pm 2.3\,(\text{isospin})) \times 10^{-10}\,,$$

where the first error is statistical, the second is systematic, and the third arises from isospin violation.

This result can be compared to those from previous τ [2] and e^+e^- experiments [35]:

$$\begin{aligned} a_\mu^{\pi\pi}[0.50, 1.80] &= (464.0 \pm 3.0\,(\text{exp.}) \pm 2.3\,(\text{isospin})) \times 10^{-10} \quad (\tau : \text{ALEPH, CLEO}) \\ a_\mu^{\pi\pi}[0.50, 1.80] &= (448.3 \pm 4.1\,(\text{exp.}) \pm 1.6\,(\text{rad.})) \times 10^{-10} \qquad (e^+e^- : \text{CMD2, KLOE})\,. \end{aligned}$$

The first error includes both statistical and experimental systematic errors added in quadrature. The second error in the e^+e^- result is due to radiative corrections. Our result agrees well with the τ-based result but is noticeably higher than the e^+e^- result. This supports the hypothesis that there is a difference between the mass spectra of the 2π systems produced in τ-decay and $e^+e^- \to \pi^+\pi^-$ reactions.

In summary, we have studied the decay $\tau^- \to \pi^-\pi^0\,\nu_\tau$ using high statistics data taken with the Belle detector at the KEKB e^+e^- collider. The branching fraction is measured with 1.2% accuracy, which is better than that in the previous experiments (except for the ALEPH result). In the unfolded $\pi^-\pi^0$ mass spectrum, in addition to the $\rho(770)$ and $\rho'(1450)$ mesons,

the production of the $\rho''(1700)$ in τ^- decays has been unambiguously demonstrated and its parameters determined. The unfolded spectrum is used to evaluate the 2π contribution to the muon anomalous magnetic moment $a_\mu^{\pi\pi}$ in the region $\sqrt{s} = 0.50 - 1.80$ GeV/c^2. Our results agree well with the previous τ based results but are higher than the e^+e^- results.

Acknowledgments

We thank M. Davier and J. H. Kühn for their advice and encouragement during this analysis. We thank the KEKB accelerator group for the excellent operation of the KEKB accelerator. We acknowledge support from the Ministry of Education, Culture, Sports, Science, and Technology of Japan and the Japan Society for the Promotion of Science; the Australian Research Council and the Australian Department of Industry, Science and Resources; the National Science Foundation of China under contract No. 10175071; the Department of Science and Technology of India; the BK21 program of the Ministry of Education of Korea and the CHEP SRC program of the Korea Science and Engineering Foundation; the Polish State Committee for Scientific Research under contract No. 2P03B 01324; the Ministry of Science and Technology of the Russian Federation; the Ministry of Education, Science and Sport of the Republic of Slovenia; the National Science Council and the Ministry of Education of Taiwan; and the U.S. Department of Energy.

[1] A. Czarnecki and W.J. Marciano, Phys. Rev. D **64**, 013014 (2001); A. Nyffeler, hep-ph/0305135 (unpublished); E. Rafael, hep-ph/0208251 (unpublished); M. Passera, J. Phys. G **31**, R75 (2005).
[2] M. Davier, S. Eidelman, A. Höcker and Z. Zhang, Eur. Phys. J. C **27**, 497 (2003).
[3] K. Hagiwara, A.D. Martin, D. Nomura, and T. Teubner, Phys. Lett. B **557**, 69 (2003).
[4] M. Davier and A. Höcker, Phys. Lett. B **435**, 427 (1998).
[5] R.R Akhmetshin *et al.* (CMD-2 Collaboration), Phys. Lett. B **578**, 285 (2004).
[6] R.R. Akhmetshin *et al.* (CMD-2 Collaboration), Phys. Lett. B **527**, 161 (2002).
[7] A. Aloisio *et al.* (KLOE Collaboration), Phys. Lett. B **606**, 12 (2005).
[8] M.N. Achasov *et al.* (SND Collaboration), hep-ex/0506076.
[9] R. Barate *et al.* (ALEPH Collaboration), Z. Phys. C **76**, 15 (1997).
[10] M. Davier, Nucl. Phys. B (Proc. Suppl.) **123**, 135 (2003).
[11] S. Anderson *et al.* (CLEO Collaboration), Phys. Rev. D **61**, 112002 (2000).
[12] K. Ackerstaff *et al.* (OPAL Collaboration), Eur. Phys. J. C **7**, 571 (1999).
[13] M. Davier, Nucl. Phys. B (Proc. Suppl.) **144**, 250 (2005).
[14] G.W. Bennett *et al.* (Muon g-2 Collaboration), Phys. Rev. Lett. **92**, 161802 (2004).
[15] Throughout this paper, the inclusion of the charge-conjugate decay mode is implied unless stated otherwise.
[16] The definition of the weak spectral function(or form factor) used in this paper ($v_-(s)$) differs by a factor of $\sqrt{2}$ from the one ($v_-^w(s)$) used in the other literature: $v_-(s)^w = \sqrt{2}v_-(s) = \sqrt{2}v_0^{I=1}(s)$. See, for example, A.Z. Dubničkova, S. Dubnička and M.P. Rekalo, Czechoslovak Jour. Phys., **43**, 1057 (1993).

[17] Using a variable x defined as

$$x = (1-\beta_\mu)/(1+\beta_\mu), \qquad \beta_\mu = (1-4m_\mu^2/s)^{\frac{1}{2}},$$

$\hat{K}(s)$ is given by

$$\begin{aligned}\hat{K}(s) &= \frac{3s}{m_\mu^2}\cdot K(s)\\ K(s) &= x^2\left(1-\frac{x^2}{2}\right)+(1+x)^2\left(1+\frac{1}{x^2}\right)\\ &\quad \left(\ln(1+x)-x+\frac{x^2}{2}\right)+\left(\frac{1+x}{1-x}\right)x^2\ln x.\end{aligned}$$

[18] S. Kurokawa and E. Kikutani, Nucl. Instr. and Meth. A **499**, 1 (2003).

[19] A. Abashian *et al.* (Belle Collaboration), Nucl. Instr. and Meth. A **479**, 117 (2002).

[20] KORALB(v2.4)/TAUOLA(v2.6): S. Jadach and Z. Wąs, Comp. Phys. Commun. **85**, 453 (1995); ibid., **64**, 267 (1991); ibid., **36**,191 (1985); S. Jadach, J.H. Kühn, and Z. Wąs, Comp. Phys. Commun. **64**, 275 (1991); ibid., **70**, 69 (1992); ibid., **76**, 361 (1993).

[21] P. Golonka *et al.*, hep-ph/0312240 (unpublished); Z. Was and P. Golonka, Nucl. Phys. Proc. Suppl. **144**, 88 (2005).

[22] The QQ B meson decay event generator was developed by the CLEO Collaboration. See http://www.lns.cornell.edu/public/CLEO/soft/QQ.

[23] S. Jadach *et al.*, Comp. Phys. Commun. **102**, 229 (1997).

[24] S. Jadach, B.H.L. Ward, Z. Wąs, Comp. Phys. Commun. **130**, 260 (2000).

[25] F.A. Berends, P.H. Daverveldt, and R. Kleiss, Comp. Phys. Commun. **40**, 285 (1986).

[26] R. Brun *et al.*, GEANT 3.21, CERN Report No. DD/EE/84-1 (1987).

[27] S. Eidelman *et al.* (Particle Data Group), Phys. Lett. B **592** 1, (2004).

[28] K. Ackerstaff *et al.* (OPAL Collaboration), Eur. Phys. Jour. C **4**, 193 (1998).

[29] S. Schael *et al.* (ALEPH Collaboration), Phys. Rep. **421**, 191 (2005).

[30] M. Acciarri *et al.* (L3 Collaboration), Phys. Lett. B **345**, 93 (1995).

[31] M. Artuso *et al.* (CLEO Collaboration), Phys. Rev. Lett. **72**, 3762 (1994).

[32] A. Höcker and V. Kartvelishvili, Nucl. Instr. Meth. A **372**, 469 (1996).

[33] G.J. Gounaris and J.J. Sakurai, Phys. Rev. Lett. **21**, 244 (1968).

[34] V. Cirigliano, G. Ecker and H. Neufeld, Phys. Lett. B **513**, 361 (2001); V. Cirigliano, G. Ecker and H. Neufeld, J. High Energy Phys. JHEP **08**, 002 (2002).

[35] M. Davier, S. Eidelman, A. Höcker, and Z. Zhang, Eur. Phys. J. C **31**, 503 (2003), A. Höcker, Proc. of the 32nd Int. Conf. on High Energy Physics (ICHEP04), Beijing, 2004, vol 2, p.710.